Nano World Journal

https://doi.org/10.17756/nwj.2023-s5-002

Research Article

Open Access

Design and Analysis of ZnO Based TFT for Detection of Hydrogen Gas

Pranaw Kumar, Tauseef Ahmed, Syed Saddique Anwer Askari and Mukul Kumar Das*

Department of Electronics Engineering, Indian Institute of Technology (ISM), Dhanbad, Jharkhand, India

***Correspondence to:**
Mukul Kumar Das
Department of Electronics Engineering,
Indian Institute of Technology (ISM),
Dhanbad, Jharkhand, India.
E-mail: mukulkdas@iitism.ac.in

Received: October 11, 2023
Accepted: December 18, 2023
Published: December 21, 2023

Citation: Kumar P, Ahmed T, Askari SSA, Das MK. 2023. Design and Analysis of ZnO Based TFT for Detection of Hydrogen Gas. *NanoWorld J* 9(S5): S07-S13.

Copyright: © 2023 Kumar et al. This is an Open Access article distributed under the terms of the Creative Commons Attribution 4.0 International License (CCBY) (http://creativecommons.org/licenses/by/4.0/) which permits commercial use, including reproduction, adaptation, and distribution of the article provided the original author and source are credited.

Published by United Scientific Group

Abstract

In this paper, zinc oxide (ZnO)-based bottom gate top contact thin film transistors (TFT) of different aspect ratio (W/L) has been investigated where the TFT's channel length (L) can be changed while maintaining a constant width (W). For the performance analysis utilizing SILVACO TCAD, we centered on the ZnO's capacity to fuse gas and the staggered inverted TFT's capability to modulate current. Analysis has been done on the effects of channel length variation, noble metals, and work function on this device structure's transfer and output characteristics. Later, the hydrogen sensing analysis was included. Here, the standard MOS gate stack is preserved in this TFT arrangement, and the source-drain terminals and channel region are covered by an ohmic gate electrode.

Keywords

Thin film transistors, Metal oxide TFTs, Zinc oxide, ATLAS

Introduction

Metal-oxide TFTs are known as an alternative to the conventional hydrogenated amorphous silicon thin film transistors (a-Si:H TFTs). TFTs provide superior performance to a-Si:H TFTs, as well as flexibility for flexible displays and good process compatibility [1, 2]. Being a kind of field effect transistor, TFTs are created by sequentially depositing thin films made of various materials. As the TFTs' active layer, semiconducting metal oxide has gained a lot of praise. Despite having several benefits, metal oxide TFTs' stability and mobility still need to be enhanced. Silicon is the semiconducting substance used in TFTs and its fabrication is expensive and complicated.

Due to large excitation energy (60 meV) of ZnO semiconductor, it has gained a remarkable attention of researchers. This large excitation energy based on excitation recombination leads to lasing action, even at room temperature. Thus finds its application in LEDs. Also, sharp transitions lead to semiconductor lasers with low threshold voltage. Anyhow, interest in ZnO is enhanced by its wide application in optoelectronic devices because of its direct wide band gap (~3.37 eV at room temperature). Also, ZnO based devices are less costly, as they have very simple crystal growth technology. Several methods have been employed to grow ZnO bulk crystal. Apart from large exciton energy and wide band gap, ZnO has more properties, which makes it superior over wide bandgap semiconductor materials. High energy radiation stability which makes it suitable for space application [3, 4].

High substitutional doping can be introduced to ZnO. By proper tailoring the level of doping, electrical properties of ZnO semiconductor can be altered [5, 6]. For both positive and negative bias, the current-voltage relationship for an ohmic contact in a device is linear and symmetric. For electrical current to flow

into and out of the semiconductor, it is essential that there be no parasitic resistance. High resistance metal- semiconductor ohmic contacts often result in device performance loss owing to thermal stress and contact failure. Therefore, ohmic connections with low resistance as well as thermal stability and dependability are of the utmost significance for high performance ZnO-based optical and electrical systems. One of the key objectives in enhancing device performance, which is crucial to device technology, should be ohmic contact metallization [7, 8].

In conjugation with transparent TFTs (TTFTs), a lot of interest has been developed for transport electronics. It is due to the wide bandgap of active layer, that TTFTs properties do not degrade as in the case of amorphous or poly Si-TFT. Hence, steps to protect the active layer from visible light is no longer required. ZnO semiconductor is considered as the most important material due to its properties like low temperature deposition, radiation tolerance and high voltage. Good quality crystalline ZnO films are grown on various substrates at low deposition temperatures [9, 10]. Physical characteristics like electronic quantum transport and enhanced radiative recombination of carriers, which emerge due to quantum confinement have drawn the attention of researchers towards one dimensional semiconductors nanowires and nanorods. Fabricated device like nano resonators, nano lasers, transducers, field effect transistors, actuators, ultrasensitive nanosized gas sensors, field emitters and nano cantilevers, which relies on one dimensional semiconductor structures have strong potential to perform in wide range [11, 12]. Hence, all these nanostructures provide a base to perform research on electron transport mechanisms in one dimensional semiconductor materials creating high-performing new generations of nano devices.

For various applications, a large number of nanowires consisting of materials like InP, Si, In_2O_3, C, SnO_2, GaN, ZnO, CdS, and GaAs have been reported using different growth methods. ZnO has resistivity to hostile environments, high electrochemical coupling constant and large exciton binding energy, which makes ZnO as one of the preferable materials among these. Since 1D ZnO structures attracted so much attention, many publications have recently been published documenting the growth of nanostructures in a variety of shapes, including nanowires, nanobelts, nanorings, nanotubes, nanodonuts, and nanopropellers, using diverse techniques [13-15].

However, elements like Al, Al_2O_3, ZnO, and other readily available materials can be used to create a non-silicon based TFT. ZnO is one of the semiconducting metal oxides that shows the most potential for TFT. The electrical, magnetic, optical, and chemical properties of ZnO are quite diverse. ZnO is used in a variety of industries, including electronics, photonics, ceramics, agriculture, and medicine [16, 17]. TTFTs have the potential to lead to the development of flexible and transportable electronics in the future [18]. Since ZnO has a large bandgap (3.37 eV), it can be used for TTFT. ZnO has a high exciton binding energy of 60 meV and functions as an n-type semiconductor material. It possesses great mobility as well as high chemical and thermal stability. It has near UV emission as well as excellent electrical conductivity, making it a preferable candidate for the active layer of oxide TFT. ZnO possesses wurzite-like hexagonal structures. Sensing characteristics, solar cells, TFTs, laser diodes, and photodetectors are among the devices that make use of this high degree of freedom in growing geometries [19]. High on/off current ratio and simplicity of fabrication characterization, makes ZnO a suitable channel material. With the exception of channel construction, the ZnO-based TFT's operating principle is quite similar to that of crystalline MOSFET devices.

To improve device performance, a number of ZnO TFT-based device architectures have been investigated [20, 21]. But there are still a number of technological issues to be solved. For instance, a high gate leakage current can be caused by a poor dielectric. Thus, it negatively impacts the interaction [22]. High threshold voltage may be caused by a high interface trap density at the semiconductor-dielectric interface. As a result, it will limit TFT functioning to high voltage [23]. Researchers have also noted that high k-dielectrics can lower leakage current and threshold voltages [24, 25]. However, it has a number of shortcomings, including a difficult manufacturing process and a rough surface. SiO_2 is easily made into a gate insulator despite having a low dielectric constant [26]. Additionally, SiO_2 is more stable than other insulators like HfO_2 and SiN_x. Atomic layer deposition [27], pulse laser deposition [28], RF sputtering [29], metal organic chemical vapor deposition [30], sol-gel method [31], thermal evaporation [32] and thermal oxidation of Zn thin films [33] are a few techniques that can be used to create the ZnO channel layer in TFTs.

Among these techniques, RF sputtering is one that is frequently used and well-liked to create ZnO thin films. Excellent Schottky contact is also formed between Pd and thin ZnO sheets [34]. Using pulse laser deposition, Ma et al., created a ZnO Schottky barrier TFT [35]. It is delineated that there is excellent field effect mobility and a high on/off current ratio. ZnO-based TFT was manufactured via RF sputtering by Montes et al. At high deposition pressure, they attained large on/off current ratios [36].

In this work, we used the SILVACO TCAD ATLAS™ module to model a ZnO-based TFT. We provide an overview of the performance analysis with an emphasis on the TFT's output current, threshold voltage, mobility, on/off current ratio, subthreshold slope, and transconductance. Source and drain electrodes made of noble metals like Pd and Au have been used for hydrogen detection. The effects of channel length, work function, and drain current on device sensitivity have all been considered as sensing parameters.

Experimentation

Modelling of TFT and theory

Generally, three terminals—the gate, source, and drain—which possess conducting, insulating, and semiconducting regions, make up a TFT. Semiconductor is positioned in between the source and drain electrodes. Between the gate and semiconductor there is a dielectric material. The current between the source and drain electrodes is directed by adjusting the gate bias, which is the fundamental working principle of TFTs. The change in gate bias takes into account the buildup of free charges at the semiconductor-dielectric interface. Fig-

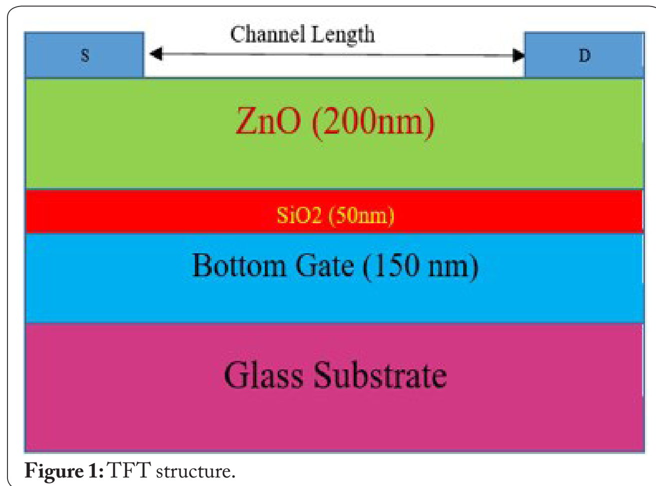

Figure 1: TFT structure.

ure 1 depicts the TFT structure that was simulated for this article. It has a bottom gate configuration and is a conventional top contact inverted staggered TFT. By maintaining the width constant, a variation in channel length is made to the TFT structure. TFT structures with top gate bottom contacts are fairly simple to manufacture.

However, bottom gate top contact has higher on/off current ratio, better mobility and better drain current characteristics. This is because bottom gate top contact (metal semiconductor) connections have lower resistance than bottom gate bottom contact devices at the source and drain contacts. To obtain an accurate electrical and sensory characterization of the device, it is possible to include this special feature of the bottom gate top contact. First of all, ZnO-based TFT's channel length has been changed to vary the aspect ratio (W/L) from 4 to 1. For all TFT structures, 180 µm of width is used. Table 1 shows the different channel lengths. Table 2 presents material properties of channel material for SILVACO TCAD.

ZnO thin film makes up the semiconductor channel layer.

Table 1: Channel dimension of TFT.

TFT structure	Channel length (in µm)	Channel width (in µm)	W/L ratio
A	45	180	4
B	60	180	3
C	90	180	2
D	180	180	1

Table 2: Material properties of channel material for SILVACO TCAD.

Simulation parameters	Properties
DOS at the conduction band edge, N_C	4.45 x 10^{18} cm^{-3}
DOS at the valance band edge, N_V	7.15 x 10^{19} cm^{-3}
Low field mobility of holes (μ_P)	10 cm^2/Vs
Low field mobility of electrons (μ_N)	60 cm^2/Vs
Affinity, ς	4.35 eV
Permittivity, εs	8.5
Capture rate for photontransition	6.41 x 10^{-14} $cm^{-3}sec^{-1}$
Band gap, Eg	3.37 eV
Shockley-Read-Hall recombination lifetime for electrons and holes (τ_N) and (τ_P)	10^{-9} s
Auger recombination rate	10^{-31} cm^6/s

Between the aluminum bottom gate and semiconductor, the dielectric SiO_2 is located. Contacts for the source and drain are similarly constructed of aluminum. The source and drain electrodes are 5 µm in width and 10 nm in length. The thickness of the bottom gate is 150 nm. As previously mentioned, TFT performance may be modeled and investigated similarly to MOSFET. Now, channel conductance is influenced by gate voltage, and it regulates whether this conductivity is ON or OFF. For an n-channel TFT, the gate and the drain voltage both have an impact on the current flowing from the drain to the source. The I-V characteristics of an n-channel TFT can be analyzed by the equation below [37]:

$$I_D = \frac{1}{2}\mu_n C_{ox}\frac{W}{L}\left[2(V_G - V_{Th})V_D - V_D^2\right] \quad \text{for } 0 \le V_D \le (V_G - V_{Th}) \qquad (1)$$

$$I_D = \frac{1}{2}\mu_n C_{ox}\frac{W}{L}(V_G - V_{Th})^2 \quad \text{for } V_D > (V_G - V_{Th}) \qquad (2)$$

Where, C_{ox} is dielectric capacitance/unit area, μ_n is the field effect mobility, W is width of the channel, L indicates channel length and V_{Th} indicates the threshold voltage which is the bare minimum gate voltage required to establish a route of conductivity between the source and drain.

Values for variables like field effect mobility, threshold voltage, transconductance, on/off current ratio, and subthreshold slope have been calculated from the I_D vs V_{GS} plot depending on the semiconductor morphology and device shape. On the basis of the plot when the device is operating in the saturation region, these parameters have been evaluated and the I_D follows the relation stated in equation 2.

Now, the on/off current ratio, which may be deduced from the I_D vs V_{GS} relation, is defined as the ratio of highest to minimum I_{DS}. It establishes the typical properties of electronic switching. ON current refers to the ability to drive. Leakage current is indicated by low off current. A higher I_{on}/I_{off} ratio is preferred for the device to operate smoothly. The threshold voltage is the V_{GS} for which there is a significant charge accumulation at the semiconductor-dielectric interface (V_T). Using a linear extrapolation of the I_D - V_{GS} relation at low V_{DS} is one of the potential approaches for calculating the V_T. Another important performance parameter is subthreshold swing which also affects TFT performance. It displays the controllability of the device's gate terminal. Additionally, it displays the V_{GS} needed to raise I_{DS} by a decade. The relationship shown in equation 3 can be used to obtain this.

$$SS = \left(\left. \frac{d\log(I_{DS})}{dV_{GS}} \right|_{\max} \right)^{-1} \qquad (3)$$

The 'SS' should always be smaller, and the results are high speed and low power consumption.

Mobility has a direct impact on switching speed and the maximum I_{DS}. Utilizing transfer characteristics, mobility can be determined. It can be calculated by using equation 4 [38].

$$\mu_{FE} = \frac{\frac{dI_D}{dV_{GS}}}{\frac{1}{2} C_{ox} \frac{W}{L} V_{DS}} \quad (4)$$

Here, the field effect mobility at low V_{DS} ($V_{DS} = 0$, $V_{DS} << V_T$) is called linear field effect mobility.

Results and Discussion

By applying the suitable material properties listed in table 1 and solving the continuity and poison equations, the impact of various channel lengths is investigated. For ATLAS™ simulation work, a fully coupled Newton method and constant low field mobility model are used. At gate voltage (V_{GS}) equal to 8 V, output characteristics (I_{DS} - V_{DS}) at different channel lengths are displayed in figure 2. The I_{DS} current (source to drain) indicated a noticeable increase with an increase in V_{DS} at positive gate voltage ($V_{GS} > 0$). This demonstrates the n-type nature of the channel.

Additionally, a very low value of drain current flows when the gate voltage is zero ($V_{GS} = 0$). This indicates that the device is in enhancement mode. The fact that each I_{DS} curve is flat at high V_{DS} indicates stiff saturation of drain current in the simulated ZnO-based TFTs. Additionally, pinch off and current saturation are both observed. It implies that the free electrons could be completely removed from the channel region, which is needed for circuit implications.

At a drain voltage (V_{DS}) of 1 V, the input characteristics of TFTs are depicted in figure 3. The threshold voltage has been calculated from the plot shown in figure 3. Figure 4 shows the transfer characteristics in logarithmic scale.

Table 3 reports the ZnO-based TFTs' acquired threshold voltage and other parameters for various channel lengths. Additionally, all of these obtained results have been compared to earlier work as shown in table 4.

Now, due to their high ratio of surface to bulk, great sensitivity, long-lasting stability, and quick reaction, metal- oxide based sensors are exceptional at detecting gases. The interaction of gas molecules with the semiconductor surface changes the surface's concentration of charge carriers. It consequently modifies the device conductance. Since hydrogen is a reducing gas, a device's behavior in its presence can be employed as a gas marker for gas detections by observing changes in the electrical properties of noble metals. This must be utilized as a key in the simulation strategy to establish a connection between the sensing equipment and the gas. Figure 5 illustrates how I_{DS} rises with V_{DS}. Additionally, with a V_{GS} of 8 V, V_{DS} can range from 0 to 16 V.

When Au is taken as the source and drain electrodes in a ZnO-based TFT, the response of the drain current is higher than when Pd is used. The increase in drain current (sensing current) is caused by hydrogen. As the concentration of target gas molecules increases, the Pd/Au electrode's work function alters. This change was caused by the hydrogen dipole concentration at the Au/Pd-ZnO interface. This contact facilitates the transfer of electrons from electrodes to a ZnO channel by creating an electric field. The energy barrier between the electrode and the thin ZnO layers is subsequently decreased due to absorption of hydrogen gas as shown in figure 6. Increasing drain current is seen as noble metals' work function declines. The decrease in work function and rise in drain current, are both caused by the formation of a hydrogen dipole at the noble metal- semiconducting oxide interface at a constant channel length of 180 µm.

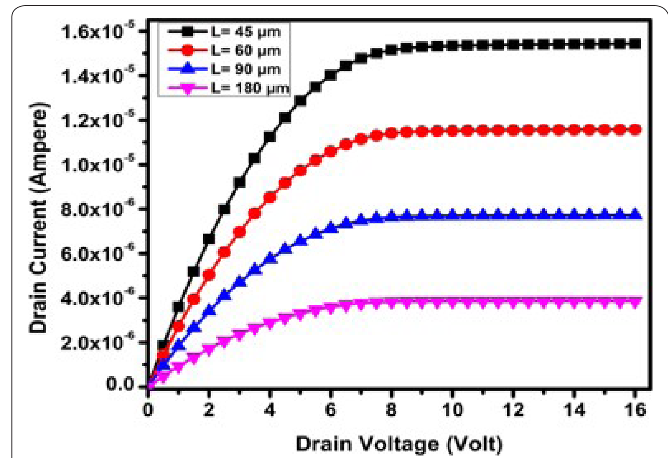

Figure 2: Output characteristics of TFTs at different channel lengths.

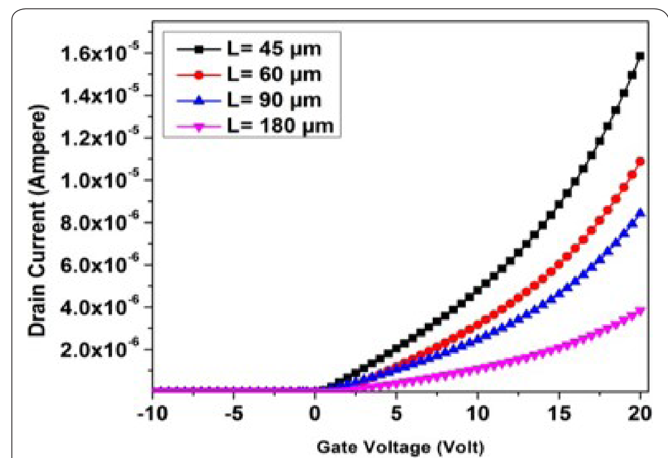

Figure 3: Input characteristics of TFTs at different channel lengths.

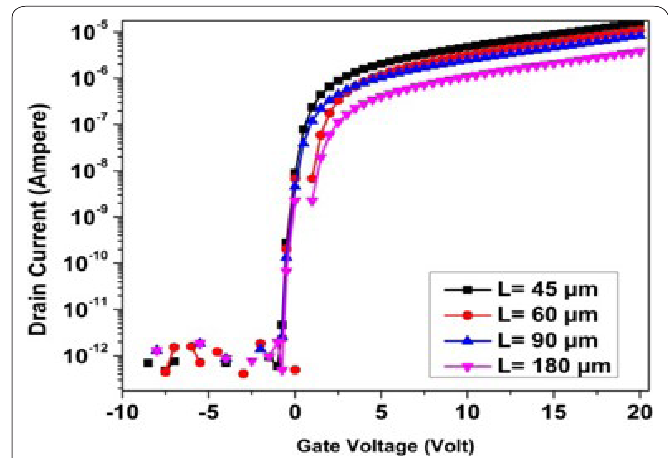

Figure 4: I_D vs V_{GS} in logarithmic scale.

Table 3: Obtained parameters of all TFT structures of this work.

TFT structure	Threshold voltage (V_{th}) (in Volts)	Field effectmobility (μ_{FE}) (in cm²/V-s)	Sub- thresholdslope (in Volts/dec)	Transconductance (g_m) (in μS)	$I_{ON/OFF}$ ratio
A	0.569	1.3845	0.96	0.319	10^6
B	0.674	1.6024	0.97	0.239	10^6
C	0.881	1.9699	0.97	0.160	10^6
D	1.3847	2.4138	0.54	0.105	10^7

Table 4: Comparison with previous work.

Parameters				Ref.
Mobility μ (cm²/V s)	Threshold voltage V_{th} (V)	On-Off ratio	Sub- threshold slope SS (V/dec)	
1.3	-	10^6	0.5	[39]
0.6134	3.1	10^2	-	[40]
2.317	1.39	6.5 x 10^6	0.3	[41]
2.4138	1.3847	10^7	0.54	[Our work]

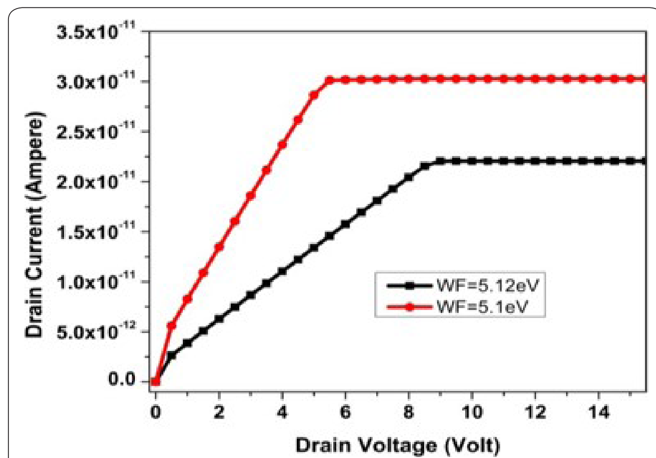

Figure 5: I_D vs V_{DS} plot of Pd and Au source/drain contact of TFT of channel length = 180 μm.

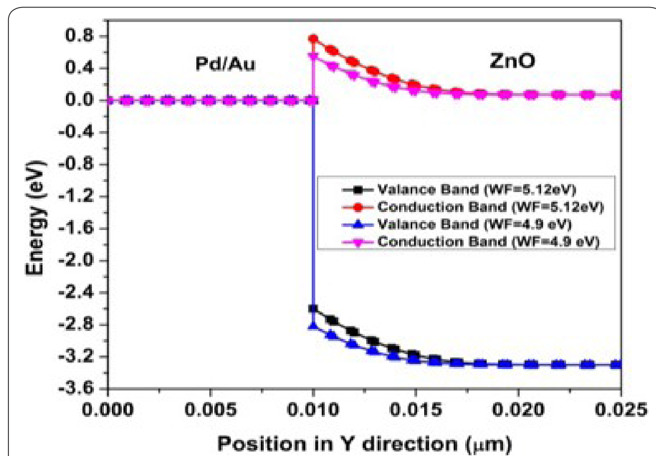

Figure 6: During the absorption of hydrogen gas, changes in the energy barrier between the Au/Pd electrodes and the thin ZnO sheet were observed.

Table 5 shows how the two different noble metals' perceived current (output characteristics) changed over time.

Table 5: Detection of sensing current (output characteristics) variation for the two noble metals (Pd and Au).

Output characteristics (at V_{GS} = 8 V), Sensing current (in A)	
Channel length (L = 180 μm)	
Pd (S/D) electrode, I_{Pd} (in A)	Au (S/D) electrode, I_{Au} (in A)
3.1 x 10^{-11}	1.9 x 10^{-11}

Table 6: Detection of sensing current (transfer characteristics) variation due to different work function at various channel length.

Transfer characteristics (V_{DS} = 1 V), Sensing current (A)		
Channel length, L (in μm)	In air, Φ_{Pd} = 5.12 eV	In H_2, Φ_{Pd} = 4.9 eV
180	3.868 x 10^{-12}	1.616 x 10^{-8}
90	3.866 x 10^{-12}	1.6145 x 10^{-8}
60	3.864 x 10^{-12}	1.612 x 10^{-8}
45	3.863 x 10^{-12}	1.606 x 10^{-8}

Table 6 shows the variation in sensing current for different channel lengths and work functions for transfer characteristics.

Conclusions

Using numerical simulation, ZnO-based TFTs with different channel lengths have been studied. The essential parameters derived from this work are shown in table 3 and the same have been compared with earlier work in table 4. Table 3 and table 4 results may change for a variety of reasons, including the use of different materials, dimensions, deposition methods, ZnO active layer flaws, and source drain contact resistance. Noble metals like Pd and Au have been studied as sources and drain electrodes for hydrogen detection. These noble metals make it easier for the ATLAS simulation to incorporate hy-

drogen sensitivity, solubility, and selectivity. The effect of channel length, drain current and impact of work function on device sensitivity have all been used as sensing parameters.

Acknowledgements

None.

Conflict of Interest

None.

References

1. Nishii J, Hossain FM, Takagi S, Aita T, Saikusa K, et al. 2003. High mobility thin film transistors with transparent ZnO channels. *Jpn J Appl Phys* 42(4A): L347. https://doi.org/10.1143/JJAP.42.L347
2. Hossain FM, Nishii J, Takagi S, Sugihara T, Ohtomo A, et al. 2004. Modeling of grain boundary barrier modulation in ZnO invisible thin film transistors. *Physica E Low Dimens Syst Nanostruct* 21(2-4): 911-915. https://doi.org/10.1016/j.physe.2003.11.149
3. Ohshima E, Ogino H, Niikura I, Maeda K, Sato M, et al. 2004. Growth of the 2-in-size bulk ZnO single crystals by the hydrothermal method. *J Cryst Growth* 260(1-2): 166-170. https://doi.org/10.1016/j.jcrysgro.2003.08.019
4. Polyakov AY, Smirnov NB, Govorkov AV, Kozhukhova EA, Vdovin VI, et al. 2003. Proton implantation effects on electrical and recombination properties of undoped ZnO. *J Appl Phys* 94(5): 2895-2900. https://doi.org/10.1063/1.1597944
5. Dietl T, Ohno OH, Matsukura AF, Cibert J, Ferrand ED. 2000. Zener model description of ferromagnetism in zinc-blende magnetic semiconductors. *Science* 287(5455): 1019-1022. https://doi.org/10.1126/science.287.5455.1019
6. Pearton SJ, Abernathy CR, Thaler GT, Frazier RM, Norton DP, et al. 2004. Wide bandgap GaN-based semiconductors for spintronics. *J Condens Matter Phys* 16(7): R209. https://doi.org/10.1088/0953-8984/16/7/R03
7. Iliadis AA, Vispute RD, Venkatesan T, Jones KA. 2002. Ohmic metallization technology for wide band-gap semiconductors. *Thin Solid Films* 420: 478-486. https://doi.org/10.1016/S0040-6090(02)00834-9
8. Ishikawa H, Tsukui K, Koide Y, Teraguchi N, Tomomura Y, et al. 1996. Effects of surface cleaning on electrical properties for Ni contacts to p-type ZnSe. *J Vacuum Sci Technol B* 14(3): 1812-1818. https://doi.org/10.1116/1.588561
9. Nomura K, Ohta H, Takagi A, Kamiya T, Hirano M, et al. 2004. Room-temperature fabrication of transparent flexible thin-film transistors using amorphous oxide semiconductors. *Nature* 432(7016): 488-492. https://doi.org/10.1038/nature03090
10. Ohya Y, Niwa T, Ban T, Takahashi Y. 2005. Rectifying properties of oxide semiconductor heterostack films at elevated temperatures. *J Solgel Sci Technol* 33: 323-326. https://doi.org/10.1007/s10971-005-6383-x
11. Wang ZL. 2004. Nanostructures of zinc oxide. *Mater Today* 7(6): 26-33. https://doi.org/10.1016/S1369-7021(04)00286-X
12. Pan ZW, Dai ZR, Wang ZL. 2001. Nanobelts of semiconducting oxides. *Science* 291(5510): 1947-1949. https://doi.org/10.1126/science.1058120
13. Roy VA, Djurišić AB, Chan WK, Gao J, Lui HF, et al. 2003. Luminescent and structural properties of ZnO nanorods prepared under different conditions. *Appl Phy Lett* 83(1): 141-143. https://doi.org/10.1063/1.1589184
14. Yu SF, Yuen C, Lau SP, Park WI, Yi GC. 2004. Random laser action in ZnO nanorod arrays embedded in ZnO epilayers. *Appl Phy Lett* 84(17): 3241-3243. https://doi.org/10.1063/1.1734681
15. Qiu Z, Wong KS, Wu M, Lin W, Xu H. 2004. Microcavity lasing behavior of oriented hexagonal ZnO nanowhiskers grown by hydrothermal oxidation. *Appl Phy Lett* 84(15): 2739-2741. https://doi.org/10.1063/1.1697633
16. Pearton SJ, Norton DP, Ip K, Heo YW, Steiner T. 2003. Recent progress in processing and properties of ZnO. *Superlattices Microstruct* 34(1-2): 3-32. https://doi.org/10.1016/S0749-6036(03)00093-4
17. Singh S, Thiyagarajan P, Kant KM, Anita D, Thirupathiah S, et al. 2007. Structure, microstructure and physical properties of ZnO based materials in various forms: bulk, thin film and nano. *J Phys D Appl Phys* 40(20): 6312. https://doi.org/10.1088/0022-3727/40/20/S15
18. Alias MF, Alamy HKh, Aljarrah RM. 2012. The role of thickness on the structural and electrical properties of DC magnetron sputtered nano ZnO thin films. *J Electron Dev* 14: 1178-1185.
19. Ghosh S, Rajan L. 2021. Zinc oxide thin-film transistor with catalytic electrodes for hydrogen sensing at room temperature. *IEEE Trans Nanotechnol* 20: 303-310. https://doi.org/10.1109/TNANO.2021.3068994
20. Hoffman RL, Norris BJ, Wager JF. 2003. ZnO-based transparent thin-film transistors. *Appl Phy Lett* 82(5): 733-735. https://doi.org/10.1063/1.1542677
21. Smith JT, Shah SS, Goryll M, Stowell JR, Allee DR. 2013. Flexible ISFET biosensor using IGZO metal oxide TFTs and an ITO sensing layer. *IEEE Sens J* 14(4): 937-938. https://doi.org/10.1109/JSEN.2013.2295057
22. Veda SN, Shaik H, Kumar KN, Diwakar SP, Kailash S, et al. 2020. Simulation, fabrication and characterization of zinc oxide TFT. In 4th International Conference on Electronics, Communication and Aerospace Technology, Coimbatore, Tamil Nadu, India.
23. Greve DW. 1998. Field Effect Devices and Applications: Devices for Portable, Low-power, and Imaging Systems. Prentice-Hall, Inc.
24. Carcia PF, McLean RS, Reilly MH. 2006. High-performance ZnO thin-film transistors on gate dielectrics grown by atomic layer deposition. *Appl Phy Lett* 88: 123509. https://doi.org/10.1063/1.2188379
25. Navamathavan R, Lim JH, Hwang DK, Kim B, Oh J, et al. 2006. Thin-film transistors based on ZnO fabricated by using radio-frequency magnetron sputtering. *J Korean Phys Soc* 48(2): 271-274.
26. Park JC, Lee HN. 2012. Dry etch damage and recovery of gallium indium zinc oxide thin-film transistors with etch-back structures. *Displays* 33(3): 133-135. https://doi.org/10.1016/j.displa.2012.05.001
27. Kwon S, Bang S, Lee S, Jeon S, Jeong W, et al. 2009. Characteristics of the ZnO thin film transistor by atomic layer deposition at various temperatures. *Semicond Sci Technol* 24(3): 035015. https://doi.org/10.1088/0268-1242/24/3/035015
28. Shin PK, Aya Y, Ikegami T, Ebihara K. 2008. Application of pulsed laser deposited zinc oxide films to thin film transistor device. *Thin Solid Films* 516(12): 3767-3771. https://doi.org/10.1016/j.tsf.2007.06.068
29. Yoshino Y, Makino T, Katayama Y, Hata T. 2000. Optimization of zinc oxide thin film for surface acoustic wave filters by radio frequency sputtering. *Vacuum* 59(2-3): 538-545. https://doi.org/10.1016/S0042-207X(00)00313-4
30. Wu CC, Wuu DS, Lin PR, Chen TN, Horng RH. 2010. Realization and manipulation of ZnO nanorod arrays on sapphire substrates using a catalyst-free metalorganic chemical vapor deposition technique. *J Nanosci Nanotechnol* 10(5): 3001-3011. https://doi.org/10.1166/jnn.2010.2171
31. Natsume Y, Sakata H. 2000. Zinc oxide films prepared by sol-gel spin-coating. *Thin Solid Films* 372(1-2): 30-36. https://doi.org/10.1016/S0040-6090(00)01056-7
32. Periasamy C, Prakash R, Chakrabarti P. 2010. Effect of post annealing on structural and optical properties of ZnO thin films deposited by vacuum coating technique. *J Mater Sci Mater Electron* 21: 309-315. https://doi.org/10.1007/s10854-009-9912-5

33. Al-Heniti SH. 2010. Growth and properties of aligned ZnO nanowires and their applications to n-ZnO/p-Si heterojunction diodes. *J Nanosci Nanotechnol* 10(10): 6606-6611. https://doi.org/10.1166/jnn.2010.2545
34. Rajan L, Chinnamuthan P, Krishnasamy V, Sahula V. 2016. An investigation on electrical and hydrogen sensing characteristics of RF sputtered ZnO thin-film with palladium Schottky contacts. *IEEE Sens J* 17(1): 14-21. https://doi.org/10.1109/JSEN.2016.2620185
35. Ma AM, Gupta M, Chowdhury FR, Shen M, Bothe K, et al. 2012. Zinc oxide thin film transistors with Schottky source barriers. *Solid State Electron* 76: 104-108. https://doi.org/10.1016/j.sse.2012.05.005
36. Medina-Montes MI, Lee SH, Pérez M, Baldenegro-Pérez LA, Quevedo-López MA, et al. 2011. Effect of sputtered ZnO layers on behavior of thin-film transistors deposited at room temperature in a nonreactive atmosphere. *J Electron Mater* 40: 1461-1469. https://doi.org/10.1007/s11664-011-1608-y
37. Ghosh S, Rajan L, Varghese A. 2022. Junctionfree gate stacked vertical TFET hydrogen sensor at room temperature. *IEEE Trans Nanotech* 21: 655-662. https://doi.org/10.1109/TNANO.2022.3217652
38. Jain N, Singh K, Sharma SK, Kumawat R. 2022. Analog/RF performance analysis of a-ITZO thin film transistor. *Silicon* 14(15): 9909-9023. https://doi.org/10.1007/s12633-021-01601-7
39. Su NC, Wang SJ, Huang CC, Chen YH, Huang HY, et al. 2010. The role of high-κ TiHfO gate dielectric in sputtered ZnO thin-film transistors. *Jpn J Appl Phys* 49(4S): 04DA12. https://doi.org/10.1143/JJAP.49.04DA12
40. Singh S, Chakrabarti P. 2012. Simulation, fabrication and characterization of ZnO based thin film transistors grown by radio frequency magnetron sputtering. *J Nanosci Nanotechnol* 12(3): 1880-1885. https://doi.org/10.1166/jnn.2012.5194
41. Hsu MH, Chang SP, Chang SJ, Wu WT, Li JY. 2018. Amorphous indium titanium zinc oxide thin film transistor and impact of gate dielectrics on its photo-electrical properties. *ECS J Solid State Sci Technol* 7(7): Q3049. https://doi.org/10.1149/2.0071807jss